

Phonon-assisted magnetic Mott-insulating state in the charge density wave phase of single-layer 1TNbSe₂

Matteo Calandra

Sorbonne Université, CNRS, Institut des Nanosciences de Paris, UMR7588, F-75252, Paris, France

We study the structural, electronic and vibrational properties of single-layer 1TNbSe₂ from first principles. Within the generalized gradient approximation, the 1T polytype is highly unstable with respect to the 2H. The DFT+U method improves the stability of the 1T phase, explaining its detection in experiments. A charge density wave occurs with a $\sqrt{13} \times \sqrt{13}$ $R30^\circ$ periodicity, in agreement with STM data. At $U = 0$, the David-star reconstruction displays a flat band below the Fermi level with a marked $d_{z^2-r^2}$ orbital character of the central Nb. The Hubbard interaction induces a magnetic Mott insulating state. Magnetism distorts the lattice around the central Nb atom in the star, reduces the hybridization between the central Nb $d_{z^2-r^2}$ orbital and the neighbouring Se p-states and lifts in energy the empty $d_{z^2-r^2}$ flat band becoming non-bonding. This cooperative Jahn-Teller and correlation effect amplifies the Mott gap. Our results are relevant for the broad class of correlated insulator in the presence of a strong Jahn-Teller effect.

PACS numbers: 75.70.Tj 71.45.Lr

The 2H polytypes of transition metal dichalcogenides (TMDs) like 2HNbSe₂, 2HTaS₂ or 2HTaSe₂, are ideal materials to study the interplay of superconductivity and charge-density wave (CDW) [1], as the electron-electron interaction has a minor role and metallicity survives in the CDW state. 1T polytypes, such as 1TTiSe₂, 1TTaS₂ or 1TTaSe₂, are substantially different and more critical, as in the CDW ground state the electron-electron interaction is supposed to substantially affect the electronic structure [2–4] and lead to Mott[5], Slater or magnetic insulating states and even to spin liquids [6]. While 1T-TaSe₂ is metallic at low temperature, the CDW state of 1T-TiSe₂ seems to have a very small electronic gap (0.1 eV). The nature of the low temperature state of 1T-TaS₂ is still very controversial as it has been proposed to be a Mott insulator[5], an Anderson disordered insulator[4] or, more recently, a metal[7].

The electronic structure of high-T phase of 1T polytypes in the absence of a CDW, (hereby labeled high-symmetry structure) can be understood, to some extent, by neglecting interlayer coupling and invoking the crystal-field symmetry around the transition metal (TM)[8, 9]. The chalcogene atoms form a slightly distorted octahedron around the TM, as shown in Fig.1 (a). In the case of an undistorted octahedron, the atomic d-levels are splitted into triply degenerate t_{2g} orbitals ($d_{x^2-y^2}$, $d_{z^2-r^2}$, d_{xy}) and doubly degenerate e_g orbitals (d_{xy} , d_{xz}) at higher energy. The distortion of the octahedron breaks the degeneracy of the t_{2g} manifold and lowers the energy of the $d_{z^2-r^2}$ orbital. For the case of Ta or Nb, the nominal d^1 valence leads to an half-filled $d_{z^2-r^2}$ state at zone center (see Fig. 1(b)), with the exact position of the Fermi level depending on the hybridization between the chalcogene and the TM orbitals.

In the case of a $\sqrt{13} \times \sqrt{13}$ $R30^\circ$ CDW with the formation of a so-called David star clustering, each one of the 13 $d_{z^2-r^2}$ states involved in the star carries one elec-

tron, leading to a formally half-filled HOMO molecular state. The narrowness of the HOMO state, related to the weaker inter-star interaction, is prone to electronic instabilities. Indeed it has been suggested[5] that bulk 1TTaS₂ is a Mott insulator. The experimental validation of this scenario in 1TTaS₂ has proven to be very controversial mainly due to the experimental incertitude in the determination of the interlayer stacking[10–13] and the consequent orbital ordering affecting hopping along the c -axis. Moreover, the occurrence of Jahn-Teller distortion within $\sqrt{13} \times \sqrt{13}$ $R30^\circ$ pattern emerging from the stabilization of a spin 1/2 magnetic state on each star has never been discussed. Finally, recent ARPES experiments[7] display a metallic band dispersion along k_z , meaning that the ground state of 1TTaS₂ is still very controversial.

The validity of the Mott scenario could be addressed by synthesizing 1TTaS₂ single-layers, however this attempt has been, for the moment, unsuccessful as (i) single-layer TaS₂ grown epitaxially on Au(111) assumes the 2H polytype[14] and (ii) preliminary results on exfoliated suspended samples seems to show that 1TTaS₂ single-layer undergoes a different kind of CDW order[15]. Although some supported samples shows Raman spectra consistent with a $\sqrt{13} \times \sqrt{13}$ $R30^\circ$ CDW [16], nothing is known on the nature of their electronic structure.

A way out of this impasse is to consider 1TNbSe₂ single-layer. Although in bulk form and in most exfoliated samples NbSe₂ assumes the 2H polytype, it has been recently shown that single-layer of 1T polytype can be grown epitaxially on bilayer graphene[17], keeping the substrate at temperatures larger than 500 K. Scanning tunneling spectroscopy shows the occurrence of a $\sqrt{13} \times \sqrt{13}$ $R30^\circ$ CDW. ARPES and STS measurements in the CDW phase seems to show the occurrence of an $\approx 0.3 - 0.4$ eV gap at zone center. No measurements of the band structure in other regions of the Brillouin

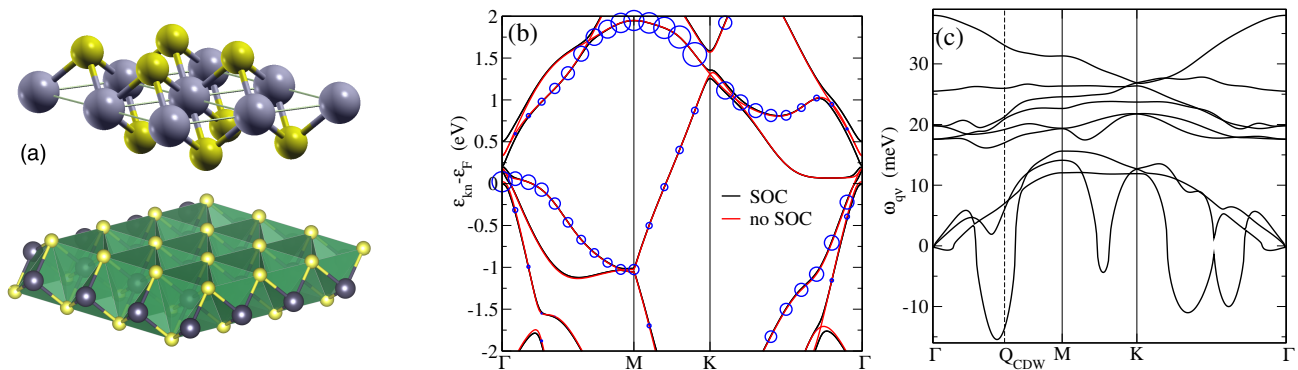


FIG. 1. (a) Crystal structure of an undistorted 1TNbSe₂ single-layer (Nb atoms in grey, Se atoms in yellow). In the bottom picture the octahedral coordination around the Nb atom is shown. Electronic structure (b) and phonon dispersion (c) of single-layer 1TNbSe₂ in the high-symmetry phase. In (b) SOC (noSOC) means with (without) inclusion of spin-orbit coupling. In the non-relativistic case, the size of the blue dots is proportional to the 3d_{z²-r²} orbital component (at Γ the larger dot correspond to 53% d_{z²-r²} component).

zone are at the moment available. Not surprisingly, the ARPES data in the CDW phase are in stark disagreement with electronic structure calculations in the high symmetry 1TNbSe₂ phase[17]. Finally, and most interesting, Bischoff *et al.*[18] recently showed that it is possible to transform the surface of exfoliated 2HNbSe₂ samples into a 1TNbSe₂ phase by applying STM bias pulse of 4V for 100 ms. The 1TNbSe₂ phase in the top layer is then (meta)stable at 77 K and displays the occurrence of the characteristic $\sqrt{13} \times \sqrt{13}$ R30° reconstruction.

In this work, by using electronic structure calculations[19, 20], we show that single-layer 1TNbSe₂ undergoes a CDW instability with a $\sqrt{13} \times \sqrt{13}$ R30° reconstruction, in agreement with experiments. A cooperative correlation and Jahn-Teller effect stabilizes a spin-1/2 magnetic Mott-insulating state in reduced dimension.

We first consider the high-symmetry 1TNbSe₂ structure shown in Fig.1. We use the in-plane experimental lattice parameter ($a_{\text{Exp.}} = 3.44\text{\AA}$) and minimize the internal coordinates. More technical details are given in the supplemental materials[21]. The calculated electronic structure shown in Fig. 1 (b) is similar to that of the undistorted 1TTaS₂ monolayer[4], however the hybridization between chalcogene and TM d-orbitals is much stronger in this case so that the bottom of the d_{z²-r²} band is substantially lower in energy and there is no gap between Nb d and Se p states. Finally, as the 1T structure breaks inversion symmetry, we carry out a fully relativistic electronic structure calculation, but we found the spin-orbit coupling to be negligible for the undistorted phase, as shown in Fig. 1 (b). For this reason we neglect relativistic effects in the rest of the paper.

We calculate the vibrational properties of the high symmetry 1TNbSe₂ phase and, not surprisingly, we find strongly unstable phonon modes (Fig. 1 (c)) with the largest instability very close to the ordering vector,

$\mathbf{Q}_{\text{CDW}} = 2\pi/\sqrt{13}a(1, 0)$, that is the nearest vector along ΓM compatible with a $\sqrt{13} \times \sqrt{13}$ distortion (see Ref. [22], Fig. 1 right). We then consider a $\sqrt{13} \times \sqrt{13} R30^\circ$ supercell and perform structural optimization assuming a non-magnetic state. We obtain the David-star structure depicted in Fig. 2 and reported in the supplemental materials[21]. The structure has three inequivalent Nb sites, central (red), hexagonal site belonging to the $\sqrt{7} \times \sqrt{7}$ cluster (blue) and peripheral (grey). The energy gain of the CDW structure with respect to the non-magnetic high-symmetry 1T structure is very large (4.2 mRyd/Nb), however the CDW structure is still substantially disfavoured from the 2H high-symmetry structure (see Tab. I). Thus, on the basis of non-magnetic calculations, it would be very difficult to detect any 1TNbSe₂ polytype.

Despite the large number of atoms in the cell, the electronic structure at the Fermi level is fairly simple. The top of the valence band is at zone center and is composed mostly of Se states originating from all the chalcogenes in the star. At the Fermi level, there is a very flat band having a marked d_{z²-r²} character from the central Nb atom (red dots in Fig. 3). The band has several avoided crossings due to the reduced symmetry of the CDW state. As it will be soon clear, tracking the central-atom d_{z²-r²} orbital-component allows to detect the upper and lower Hubbard bands.

The narrowness of the band suggests the possible occurrence of electronic instabilities. Then, in an effort to stabilize a magnetic state, we perform a spin-polarized generalized gradient approximation on top the GGA[23] non-magnetic geometry. However, we always converge to a non-magnetic state. We then consider the GGA+U approximation as implemented in Ref. [24]. We calculate the Hubbard U self-consistently [25] and obtain $U = 2.95$ eV, slightly larger of what has been obtained in 1TTaS₂ [4]. We then perform magnetic calculations within this

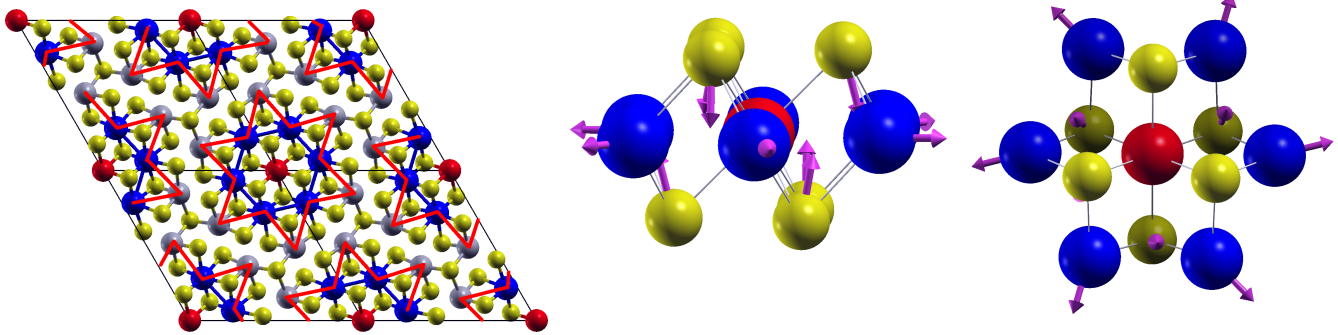


FIG. 2. Left: Optimized crystal structure for the low temperature phase of 1TNbSe_2 . There are three inequivalent Nb sites: central Nb (red), hexagonal site belonging to the $\sqrt{7} \times \sqrt{7}$ cluster (blue) and peripheral Nb sites (grey). The Se atoms are shown in yellow. The red line is a guide to the eye to recognize the $\sqrt{13} \times \sqrt{13}$ cluster (David star). The inclusion of the Hubbard term leads to a ferromagnetic state with an important local distortion around the central Nb atom in the star. However the difference between the ferromagnetic and non-magnetic structures are not visible on this scale. The magnetic state has a total magnetization of $+1\mu_B$. The magnetic moments on Nb atoms are: $0.58\mu_B$ central (red) Nb, $0.0417\mu_B$ blue Nb, $-0.0256\mu_B$ peripheral (grey) Nb. The moduli of the magnetic moments on Se atoms are smaller than $0.08\mu_B$. Center and left: magnetic induced distortion (side and top views) in the central $\sqrt{7} \times \sqrt{7}$ cluster. The central atom is unshifted. The 6 blue Nb atoms interacting ferromagnetically with the central one, moves apart in-plane. The out-of-plane Se approaches the Nb basal plane. In the top view (rightmost panel) the bottom Se atoms are shown in a darker yellow color.

approximation. We now find that the ground state of single-layer 1TNbSe_2 in the $\sqrt{13} \times \sqrt{13} R30^\circ$ phase is ferromagnetic with a total spin magnetization of $1\mu_B$ per cell and an absolute magnetization (sum of the modulus of the magnetic moments on all atoms in the cell) of $2.2\mu_B$.

Before proceeding further, it is very instructive to consider the effect of the Hubbard correction and of the stabilization of a magnetic state on the energetics of the different polytypes of single-layer NbSe_2 . Complete structural optimization within the GGA+U method leads to cell parameters in excellent agreement with experimental data even for what concerns the 2H non-magnetic high-symmetry structure (see Tab. I), with essentially no change in its electronic structure (see [21]). The GGA+U corrects the GGA underbinding error. The energy differences between the non-magnetic 1T and 2H high-symmetry structures is still large, but substantially reduced, suggesting that the high-symmetry 1T phase cannot be easily stabilized. The only effect of the GGA+U approximation on the electronic structure of high-symmetry phase of single layer 1TNbSe_2 is to unmix Se p and Nb d states at the Fermi level at zone center (see [21]). Most important, the total energy of the magnetic $\sqrt{13} \times \sqrt{13} R30^\circ$ structure has a 1.6 mRyd energy gain with respect to the 2HNbSe_2 high-symmetry structure. The 1TbSe_2 CDW phase is comparable in energy with the high symmetry structure. Thermal or cinetic effects stabilize then one or the other at 500 K.

In order to compare different approximations for the exchange correlation functional on the electronic structure, we stick to the the experimental cell parameter,

as cell relaxation is anyway marginal. We disentangle the magnitude of the Hubbard term from the magnetic-induced structural distortion by first calculating the electronic structure within the GGA+U approximation on top of the GGA geometry. A ferromagnetic state is stabilized even in this case with opening of an Hubbard gap between the majority and minority bands having dominant $d_{z^2-r^2}$ character on the central Nb atom, as shown in Fig. 3 (see filled and open red dots in the center panel). However, the electronic structure is still metallic due to the residual hybridization between the $d_{z^2-r^2}$ central Nb and the nearest neighbours Se atoms.

Structural optimization of internal coordinates within the GGA+U approximation in the magnetic state leads to a substantial distortion of the $\sqrt{7} \times \sqrt{7}$ cluster around the central Nb (i.e. the 6 Nb atoms in blue in Fig. 2 , left). If the GGA+U approximation with $U = 2.95$ eV is performed at clamped nuclei, i. e. it is carried out on the CDW structure obtained at $U = 0$ eV, the loss in total energy with respect to the fully optimized structure at $U = 2.95$ eV is ≈ 0.8 mRyd/Nb atom, corresponding to $\approx 30\%$ of the total energy gain by the CDW distortion at $U = 0$ eV (see Tab. I).

The distortion leaves unshifted the central Nb atom, while the 6 nearest Nb atoms move in-plane and apart from the central one and the out of plane Se atoms fills the empty space reducing the distance with the Nb plane, as shown in Fig. 2 (center and right). The hybridization between the central Nb $d_{z^2-r^2}$ orbital and the nearest Se p-states is reduced and the band degeneracy is removed by opening a gap in the spectrum, as in a molecular Jahn-Teller effect. The minority band with the largest

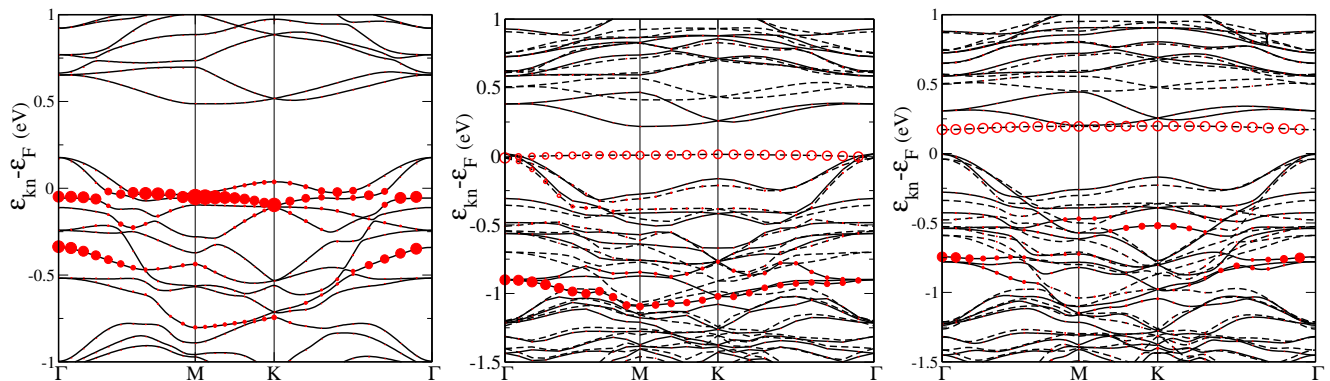


FIG. 3. Left: Electronic structure in the charge density wave phase of 1TNbSe₂ within the non-magnetic GGA. The size of the red dots is proportional to the Nb central-atom $d_{z^2-r^2}$ orbital character, (the red dot at zone center and -0.05 eV corresponds to 15% orbital character). Center: same as left but in the GGA+U approximation on top of the non-magnetic geometry. Continuous (dashed) lines are majority (minority) spin bands. The size of the full (open) dots is proportional to the Nb central-atom $d_{z^2-r^2}$ up-spin (down-spin) orbital character. Right: as in the center panel, but on top of the GGA+U geometry. The Hubbard induced distortion raises in energy the minority spin band and increases Mott gap.

Nb $d_{z^2-r^2}$ orbital component becomes non-bonding (see Fig. 3, right). The shift of the other atoms not belonging to the $\sqrt{7} \times \sqrt{7}$ cluster, is minor, so that overall the David-star CDW is preserved. More quantitatively, using the experimental lattice parameter, the distance between the central Nb atom in the star and its neighbouring Nb is $\approx 3.157\text{\AA}$ at $U = 0$ eV and $\approx 3.226\text{\AA}$ at $U = 2.95$ eV. Similarly, the distance of between Se atoms of the $\sqrt{7} \times \sqrt{7}$ cluster from the Nb-plane is decreased from $\approx 1.838\text{\AA}$ at $U = 0$ eV to 1.788\AA at $U = 2.95$ eV.

Thus, the insulating state in 1TNbSe₂ is not simply reached via a standard Mott mechanism, but a cooperative lattice and magnetic effect increases the Mott gap and amplifies the effect of the Hubbard interaction. Within GGA+U, single-layer 1TNbSe₂ is then a phonon-assisted spin-1/2 ferromagnetic Mott insulator displaying a $\sqrt{13} \times \sqrt{13}$ $R30^\circ$ David-star CDW.

It is worth to mention that our calculated gap is approximately 0.18 eV, smaller than the one detected in STM (0.3 – 0.4 eV) and ARPES in Ref. [17]. The gap does not seem to increase anymore with U , as for $U > 3.1$ eV, the flat band becomes higher in energy than the next two empty bands[21, 26]. After submission of our work, it was suggested [27] that the gap underestimation could be due to the lack of non-local exchange in the calculation. Beside this, other effects could also affect the gap size like the presence of a graphene substrate leading to a non-negligible charge transfer or band-bending occurring in STM. Nevertheless, it is important to underline that the valence band electronic structure is in good agreement with experimental data despite the large temperature broadening occurring in experiments[21].

In this work, by using first principles calculations, we have shown that single layer 1TNbSe₂ undergoes a CDW instability with a $\sqrt{13} \times \sqrt{13}$ $R30^\circ$ reconstruction. However, the GGA leads to a substantially unsta-

ble 1TNbSe₂ structure with respect to the 2H polytypes. The GGA+U approximation improves the stability of all 1T polytypes, explaining the detection of 1TNbSe₂ in experiments. Moreover, it stabilizes a ferromagnetic state with a spin magnetization of $1\mu_B$. Ferromagnetism occurs in the context of a flat d-band, as in the ferromagnetic cuprate LaBaCuO₅[28, 29]. However, while in the latter the flat band is isolated and even the LSDA stabilizes a sizeable gapped ferromagnetic state, in 1TNbSe₂ the situation is more complicated by the non-negligible hybridization with Se states at zone center and the framework is more that of a multiband Hubbard model. If the lattice is kept frozen at the non-magnetic crystal structure, then hybridization hinders the opening of a Mott gap and favours a metallic state (or a state with a negligible gap). Thus, even if to some extent the long-standing proposal of Ref. [5] based on a purely electronic mechanism partly applies to 1TNbSe₂, this is also not the complete explanation as the opening of the gap occurs via a cooperative electronic and lattice (Jahn-Teller) effect, resulting from ferromagnetism and the subsequent Nb-Nb bond-softening around the central Nb atom in the star. Even if for small values of $U < 3.1$ eV the size of the gap depends on the value of the Hubbard U parameter (that in our work is calculated from first principles self-consistently[25]), the distortion amplifies anyway the effect of the Hubbard term by reducing the hybridization (the larger U , the larger the local distortion).

We believe that the cooperative enhancement of the Mott gap due to electronic and lattice degrees of freedom is relevant far beyond the family of 1T dichalcogenides, but it is a genuine feature of correlated insulators in the presence of strong Jahn-teller distortion. A similar mechanism was suggested to be relevant in manganites and manganese oxides [30] or in the fullerenes like K₄C₆₀ [31]. 1TNbSe₂ is an ideal playground to study

Mott Jahn-Teller insulators in reduced dimension.

We acknowledge IDRIS, CINES and TGCC and PRACE for high performance computing resources, support from the European Union Horizon 2020 research and innovation programme under Grant agreement No. 696656-GrapheneCore1 and from Agence Nationale de la Recherche under the reference No. ANR-13-IS10-0003-01. We acknowledge M. Casula for useful discussions.

-
- [1] J. A., Salvo, F.J. Di and Mahajan, *Advances in Physics*, **24**, 117 (1975)
- [2] K. Rossnagel, *Journal of Physics: Condensed Matter* **23**, 213001 (2011)
- [3] R. Bianco, M. Calandra, and F. Mauri *Phys. Rev. B* **92**, 094107 (2015)
- [4] P. Darancet, A. J. Millis, and C. A. Marianetti *Phys. Rev. B* **90**, 045134 (2014)
- [5] P. Fazekas and E. Tosatti, *Physica B* **99** 183 (1980), *Philos. Mag. B* **39**, 229 (1979).
- [6] Martin Klanjek, Andrej Zorko, Rok Zitko, Jernej Mravlje, Zvonko Jaglicic, Pabitra Kumar Biswas, Peter Prelovsek, Dragan Mihailovic and Denis Arcon, *Nature Physics* **13**, 1130 (2017)
- [7] Arlette S. Ngankeu, Sanjoy K. Mahatha, Kevin Guilloy, Marco Bianchi, Charlotte E. Sanders, Kerstin Hanff, Kai Rossnagel, Jill A. Miwa, Christina Breth Nielsen, Martin Bremholm, and Philip Hofmann, *Phys. Rev B* **96**, 195147 (2017)
- [8] Myung-Hwan Whangbo and Enric Canadell, *J. Am. Chem. Soc.* **114**,9587,(1992)
- [9] L. F. Mattheiss, *Phys. Rev. B* **8**, 3719 (1973)
- [10] Albert Spijkerman, Jan L. de Boer, Auke Meetsma, Gerrit A. Wieggers, and Sander van Smaalen *Phys. Rev. B* **56**, 13757 (1997)
- [11] Tanda, S., Sambongi, T., Tani, T., and Tanaka, J. *Phys. Soc. Jpn* **53**, 476 (1984).
- [12] Nakanishi, K. and Shiba, H., *J. Phys. Soc. Jpn* **53**, 1103 (1984).
- [13] T. Ritschel, J. Trinckauf, K. Koepf, B. Chner, M. v. Zimmermann, H. Berger, Y. I. Joe, P. Abbamonte and J. Geck, *Phys. Rev. B* **71**, 153101 (2005)
- [14] C. E. Sanders, M. Dendzik, A. S. Ngankeu, A. Eich, A. Bruix, M. Bianchi, J. A. Miwa, B. Hammer, A. A. Kha-jetoorians, and P. Hofmann, *Phys. Rev. B* **94**, 081404 (2016).
- [15] D. Sakabe, Zheng Liu, Kazutomo Suenaga, Keiji Nakat-sugawa and Satoshi Tanda, *npj Quantum Materials* **2**, 22 (2017) ; doi:10.1038/s41535-017-0025-8
- [16] Albertini, O. R. *et al.*, *Phys. Rev. B* **93**, 214109 (2016)
- [17] Yuki Nakata, Katsuaki Sugawara, Ryota Shimizu, Yoshinori Okada, Patrick Han, Taro Hitosugi, Keiji Ueno, Takafumi Sato and Takashi Takahashi, *NPG Asia Materials* **8**, e321 (2016)
- [18] Felix Bischoff, Willi Auwärter, Johannes V. Barth, Agustin Schiffrin, Michael Fuhrer, and Bent Weber, *Chem. Mater.*, **29** 9907 (2017)
- [19] P. Giannozzi, S. Baroni, N. Bonini, M. Calandra, R. Car, C. Cavazzoni, D. Ceresoli, G. L. Chiarotti, M. Cococcioni, I. Dabo, A. Dal Corso, S. Fabris, G. Fratesi, S. de Gironcoli, R. Gebauer, U. Gerstmann, C. Gougous-sis, A. Kokalj, M. Lazzeri, L. Martin-Samos, N. Marzari, F. Mauri, R. Mazzarello, S. Paolini, A. Pasquarello, L. Paulatto, C. Sbraccia, S. Scandolo, G. Sciauzero, A. P. Seitsonen, A. Smogunov, P. Umari, R. M. Wentzcovitch, *J.Phys.:Condens.Matter* **21**, 395502 (2009)
- [20] P Giannozzi, O Andreussi, T Brumme, O Bunau, M Buongiorno Nardelli, M Calandra, R Car, C Cavazzoni, D Ceresoli, M Cococcioni, N Colonna, I Carnimeo, A Dal Corso, S de Gironcoli, P Delugas, R A DiStasio Jr, A Ferretti, A Floris, G Fratesi, G Fugallo, R Gebauer, U Gerstmann, F Giustino, T Gorni, J Jia, M Kawamura, H-Y Ko, A Kokalj, E Kkbenli, M Lazzeri, M Marsili, N Marzari, F Mauri, N L Nguyen, H-V Nguyen, A Otero-de-la-Rozza, L Paulatto, S Ponc, D Rocca, R Sabatini, B Santra, M Schlipf, A P Seitsonen, A Smogunov, I Timrov, T Thonhauser, P Umari, N Vast, X Wu and S Baroni, *J.Phys.:Condens.Matter* **29**, 465901 (2017)
- [21] See Supplemental materials at xxx for technical details, structural parameters, electronic structure of NbSe₂ polytypes in the high-T phase, projected density of states plots and comparison with ARPES data.
- [22] Yizhi Ge and Amy Y. Liu, *Phys. Rev. B* **82**, 155133 (2010)
- [23] Perdew, John P., Kieron Burke, Matthias Ernzerhof , *Phys. Rev. Lett.* **77**, 3865 (1996)
- [24] Matteo Cococcioni and Stefano de Gironcoli *Phys. Rev. B* **71**, 035105 (2005)
- [25] Heather J. Kulik, Matteo Cococcioni, Damian A. Scherlis, and Nicola Marzari *Phys. Rev. Lett.* **97**, 103001 (2006)
- [26] D. Pasquier and O. V. Yazyev, arXiv:1803.10727.
- [27] E. Kamil *et al.*, arXiv:1804.03898
- [28] V. Eyert *et al* *Eur. Phys. Lett.* **31**, 385 (1995)
- [29] Wei Ku, H. Rosner, W. E. Pickett, and R.T. Scalettar, *Phys. Rev. Lett.* **89**, 167204 (2002)
- [30] Y. Motome and M. Imada, *J. Phys. Soc. Jpn.* **68**, 16 (1999)
- [31] M. Fabrizio and E. Tosatti, *Phys. Rev. B* **55**, 13465 (1997)

| Structure | $\Delta E(U = 0, \text{Exp.})$ | $\Delta E(U = 2.95, \text{Exp.})$ | $\Delta E(U = 0, \text{Opt.})$ | $\Delta E(U = 2.95, \text{Opt.})$ | $a(U = 0)$ | $a(U = 2.95)$ |
|------------------|--------------------------------|-----------------------------------|--------------------------------|-----------------------------------|------------|---------------|
| 2H high-symmetry | 0.0 | 0.0 | 0.0 | 0.0 | 3.473 | 3.451 |
| 1T high-symmetry | +7.2 | +4.2 | +7.3 | +4.4 | 3.482 | 3.464 |
| 1T CDW | +3.0 | -1.1 | +2.9 | -1.6 | 12.575 | 12.523 |

TABLE I. Energetics of single-layer NbSe₂ polytypes with respect to the high-symmetry 2HNbSe₂ polytype, $\Delta E = E - E(2H)$, as a function of U . The labels $\Delta E(U = 0, \text{Exp.})$, $\Delta E(U = 2.95, \text{Exp.})$ means that the internal coordinates have been optimized at fixed volume using the experimental lattice parameters and the GGA+U functional with $U = 0$ and $U = 2.95$ eV respectively. The labels $\Delta E(U = 0, \text{Opt.})$ and $\Delta E(U = 2.95, \text{Opt.})$ refers to complete structural optimization of internal coordinates and volume using the GGA+U approximation with with $U = 0$ and $U = 2.95$ eV respectively. The energy units are mRyd per Nb atom and U is expressed in eV. The values of the experimental (Exp.) and optimized (Opt.) cell parameter are shown (in \AA). We use as experimental lattice parameter the in-plane one of the bulk, namely $a_{\text{Exp.}} = 3.44\text{\AA}$.